PARALLEL THREE-DIMENSIONAL COMPUTATION OF FLUID DYNAMICS AND FLUID-STRUCTURE INTERACTIONS OF RAM-AIR PARACHUTES

Final Report Submitted to NASA Johnson Space Center

NASA Grant Number: NASA/NAG 9-919

NASA JSC Contact Person: Fred Martin
Mail Code EG3
Tel: (281) 483-4698 Fax: (281) 244-5256

by

Tayfun E. Tezduyar
Department of Aerospace Engineering and Mechanics
107 Akerman Hall
University of Minnesota
Minneapolis, MN 55455

Tel: (612) 626-8095
Fax: (612) 626-1596
Email: tezduyar@ahpcrc.umn.edu

Date of Final Report: September 17, 1998

PARALLEL THREE-DIMENSIONAL COMPUTATION OF FLUID DYNAMICS AND FLUID-STRUCTURE INTERACTIONS OF RAM-AIR PARACHUTES

Tayfun E. Tezduyar
Department of Aerospace Engineering and Mechanics
107 Akerman Hall
University of Minnesota

1. OVERVIEW

This is a final report as far as our work at University of Minnesota is concerned. The report describes our research progress and accomplishments in development of high performance computing methods and tools for 3D finite element computation of aerodynamic characteristics and fluid-structure interactions (FSI) arising in airdrop systems, namely ram-air parachutes and round parachutes. This class of simulations involves complex geometries, flexible structural components, deforming fluid domains, and unsteady flow patterns. The key components of our simulation toolkit are a stabilized finite element flow solver, a nonlinear structural dynamics solver, an automatic mesh moving scheme, and an interface between the fluid and structural solvers; all of these have been developed within a parallel message-passing paradigm.

2. METHODS

The methods used in this project include efficient flow solvers based on the space-time finite element method and parallel computing strategies using the message-passing model,. In parachute systems, where the deformations are large, the structure is currently modeled by cable-membrane-lumped mass elements. The nonlinear response is accounted for by casting a Lagrangian description of the governing equations. In computation of fluid-structure interactions involved in parachute systems, we are increasing the sophistication of handling the coupling between the aerodynamics and the parachute deformations. Also, more sophisticated mesh generation and update methods are to be developed to handle various stages of the ram-air parachute, such as turning with unsymmetric flare. Implementation of these methods is being provided on a wide variety of architectures such as the CRAY T3E and SGI MP systems.

3. FSI SIMULATIONS AND RESULTS

In fluid-structure interactions, we developed a parallel cable-membrane structural dynamics solver. A coupling strategy for structural and flow solvers was also designed; this accommodates both nodally equivalent or incompatible meshes. The coupled solver was used to simulate a time-accurate fluid-structure interactions for a T-10 personnel parachute, and also a steady-state configuration of a ram-air parachute. In the T-10 simulations, the canopy is observed to inflate in certain regions and deflate in other regions, concurrent with the pressure fluctuations on the canopy surface due to vortex shedding. In the ram-air parachute, the initial configuration of the parachute is a smooth curved wing. Upon inflation we observe the appearance of "bumps" and a change in its spanwise curvature.

We tested our methods on time-accurate simulation of flow past round and cross parachutes at realistic conditions using unstructured meshes. The geometry for the cross parachute was obtained from researchers at Natick RDEC and the computed drag coefficients are in good agreement with

experimental results. The capability of our automatic mesh generator was enhanced to create dual surfaces on the parachute canopies, since these are required when modeling them as structural membranes. A parallel cable-membrane structural solver was developed and interfaced with a space-time based incompressible flow solver. Preliminary results for round and ram-air parachutes were obtained using the coupled solvers. In addition, stand alone structural dynamics simulations for the X-38 ram-air parafoil were conducted at the AHPCRC and Natick RDEC (with assistance from the University of Connecticut). These models are utilizing the "cut pattern" geometry of the parafoil, internal "ribs" and suspension lines.

4. PUBLICATIONS

This work resulted in the following publications. We attach copies of these articles. The work described in these articles were either directly within the scope of the class of projects under this grant, or were solved with methods and tools developed for the class of projects under this grant.

1. V. Kalro and T. Tezduyar, "A Parallel Finite Element Methodology for 3D Computation of Fluid-Structure Interactions in Airdrop Systems", *Proceedings of the 4th Japan-US Symposium on Finite Element Methods in Large-Scale Computational Fluid Dynamics*, Tokyo, Japan (1998).

2. K. Stein, R. Benney, V. Kalro, T. Tezduyar, J. Leonard and M. Accorsi, "Parachute Fluid-Structure Interactions: 3-D Computation", *Proceedings of the 4th Japan-US Symposium on Finite Element Methods in Large-Scale Computational Fluid Dynamics*, Tokyo, Japan (1998).

3. Y. Osawa, V. Kalro and T. Tezduyar, "Multi-Domain Parallel Computation of Wake Flows around Secondary Objects", *Proceedings of the 4th Japan-US Symposium on Finite Element Methods in Large-Scale Computational Fluid Dynamics*, Tokyo, Japan (1998).

4. Y. Osawa, V. Kalro, and T. Tezduyar., "A Multi-Domain Method for Computation of Long-Wake Flows", *Proceedings of the 2nd Ankara International Aerospace Conference*, Ankara, Turkey (1998).

A Parallel Finite Element Methodology for 3D Computation of Fluid-Structure Interactions in Airdrop Systems

Vinay Kalro [1] and Tayfun Tezduyar [1]

1 Aerospace Engineering and Mechanics, Army HPC Research Center
University of Minnesota, Minneapolis, Minnesota, USA
kalro@ahpcrc.umn.edu
tezduyar@ahpcrc.umn.edu

1. INTRODUCTION

We are interested in developing a fluid-structure interaction (FSI) capability which can be used for 3D simulation of airdrop systems. The systems under consideration include conventional personnel round parachutes, cross parachutes which have limited glide capability and large gliding ram-air parachutes (parafoils) which can carry upto 21 tons. The design emphasis for these systems is precision delivery when deployed under demanding conditions such as strong wind gusts and large offsets. Since conventional design techniques are time consuming, expensive and semi-empirical at best, our aim is to provide a viable, cost effective design aid based on high performance computing technology.

Parachute systems present very complex dynamics arising from interactions between the canopy, suspension lines, payload and surrounding air. Parachutes can experience significant canopy deformations and changes in orientation, even during steady-state operations. Modeling these phenomena involves a time-variant domain for the parachute system which must be accounted for in order to correctly represent the physics.

The early models developed by us [1, 2] represented the canopy and payload as a system of point masses where the deformation of the canopy was assumed to be given. In a complementary effort, Benney et al. [3] presented detailed structural analysis of parachute systems with assumed pressure distributions. Stein et al. [4] presented an axisymmetric model where the parachute was represented by cable elements, and its response was coupled to the flow field.

Our current methodology combines a stabilized space-time finite element flow solver with a cable-membrane finite element structural dynamics solver. Both solvers have been developed and interfaced within a message-passing parallel computing paradigm. The other key components in our FSI simulation toolkit are a coupling strategy between fluid and structural solver, and a mesh mover for deforming the fluid mesh based on displacements at the fluid-structure interface.

2. FLUID DYNAMICS SOLVER

2.1 Governing Equations

Let $\Omega_t^f \subset \mathbb{R}^{n_{sd}}$ be the spatial domain of interest bounded by boundary Γ_t^f at any instant "t". Here the superscript f stands for the fluid component and n_{sd} is the

number of spatial dimensions. The Navier-Stokes equations governing incompressible flows are:

$$\rho^f(\frac{\partial \mathbf{u}}{\partial t} + \mathbf{u}\cdot\nabla\mathbf{u} - \mathbf{f}) - \nabla\cdot\sigma^f = 0 \qquad \text{on } \Omega_t^f, \tag{1}$$

$$\nabla\cdot\mathbf{u} = 0 \qquad \text{on } \Omega_t^f. \tag{2}$$

Here ρ^f, $\mathbf{u}$, $\mathbf{f}$ and σ^f are the density, velocity, body force and the stress tensor, respectively. The stress tensor is written as the sum of its isotropic and deviatoric parts, and the fluid is assumed to be Newtonian. The boundary Γ_t^f is composed of $(\Gamma_t^f)_g$ and $(\Gamma_t^f)_h$ corresponding to Dirichlet- and Neumann-type boundary conditions respectively. A divergence-free velocity field is specified as initial condition. A Baldwin-Lomax turbulence model is used.

2.2 Finite Element Formulation

The flow solver is based on the Deforming-Spatial-Domain/Stabilized-Space-Time (DSD/SST) formulation [5,6] which automatically accounts for deformations in the fluid mesh. The formulation is written over individual space-time slabs, and successive time slabs are coupled in a weak sense. This allows obtaining the solution on a single space-time slab at every instant. The formulation is also stabilized to circumvent spurious oscillations due to presence of sharp boundary layers at high Reynolds number [7] and choice of velocity and pressure interpolants which otherwise violate the Babuska-Brezzi [8] condition.

3. STRUCTURAL DYNAMICS SOLVER

3.1 Governing Equations

Let $\Omega_t^s \subset I\!R^{n_{sd}}$ be the spatial domain of interest bounded by boundary Γ_t^s at any instant "t". Here the superscript s stands for the structural component. The governing equations for the structure is obtained from the conservation of linear momentum:

$$\rho^s(\frac{d^2\mathbf{x}^s}{dt^2} - \mathbf{f}) - \nabla\cdot\sigma^s = 0 \qquad \text{on } \Omega_t^s. \tag{3}$$

Here $\mathbf{x}^s$ is the structural displacement. As is the case for the fluid, the boundary Γ_s^t is composed of $(\Gamma_t^s)_g$ and $(\Gamma_t^s)_h$.

The structure undergoes large deformations leading to geometric nonlinearities. The resulting strains are assumed to be small and hence a materially linear elastic model is used. To account for the kinematic nonlinearities, the constitutive equations are written in the original undeformed configuration, in terms of the 2nd Piola-Kirchoff stress tensor $\mathbf{S}$ and the Green-Lagrange strain tensor $\mathbf{E}$. The structure is composed of cable and membrane elements. The cable elements are assumed to lie in a state of uniaxial stress:

$$S^{11} = E_c G^{11} G^{11} E_{11}. \tag{4}$$

The membrane elements are assumed to lie in a state of planar stress:

$$S^{ij} = (\overline{\lambda}_m G^{ij} G^{kl} + \mu_m [G^{il} G^{jk} + G^{ik} G^{jl}]) E_{kl}, \tag{5}$$

where

$$\bar{\lambda}_m = \frac{2\lambda_m \mu_m}{(\lambda_m + 2\mu_m)}. \tag{6}$$

Here G^{ij} are the components of the contravariant metric tensor, E_c is the modulus of elasticity for the cable, and λ_m and μ_m are the Lame parameters for the membrane. The indices i,j,k,l take on the range (1-2). For further details, the reader is referred to Bathe [9] and Po [10].

3.2 Finite Element Formulation

The finite element formulation is derived from the principle of virtual work:

$$\int_{\Omega_s^0} \rho^s \frac{d^2\mathbf{x}^s}{dt^2} \cdot \delta\mathbf{x}^s d\Omega + \int_{\Omega_s^0} \mathbf{S} : \delta\mathbf{E} d\Omega = \int_{\Gamma_t^s} \mathbf{t} \cdot \delta\mathbf{x}^s d\Gamma + \int_{\Omega_t^s} \rho^s \mathbf{f} \cdot \delta\mathbf{x}^s d\Omega. \tag{7}$$

Here $\mathbf{t}$ is the surface traction which also adds to the nonlinearity since it results in a follower force field. The left-hand-side terms in Eq. 7 are written in the original configuration. Upon discretization using appropriate function spaces, a nonlinear system of equations is obtained at each time-step. This is solved using Newton-Raphson iterations:

$$\mathbf{M}\frac{d^2\Delta\mathbf{d}^s}{dt^2} + \mathbf{C}\frac{d\Delta\mathbf{d}^s}{dt} + \mathbf{K}\Delta\mathbf{d}^s = \mathbf{R},$$
$$\mathbf{C} = \eta\mathbf{M} + \zeta\mathbf{K}. \tag{8}$$

Here $\mathbf{M}$ is the mass matrix, $\mathbf{C}$ is an artificial damping matrix which stabilizes the structural system, $\mathbf{K}$ is the stiffness matrix, $\mathbf{R}$ is the residual vector, and $\Delta\mathbf{d}^s$ is the increment in the nodal displacements. The Hilber-Hughes-Taylor [11] scheme is used for time-marching.

4. FLUID-STRUCTURE COUPLING STRATEGY

Let Γ_t^{fs} be the common boundary between the fluid and structure domains. Coupling is established by transferring velocity (and displacements) from structure to fluid, and in return traction from fluid to structure. Hence from the perspective of the flow solver, $\Gamma_t^{fs} \subset (\Gamma_t^f)_g$ and for the structural solver $\Gamma_t^{fs} \subset (\Gamma_t^s)_h$. In the current implementation only the pressure contribution to the interface traction is considered. Two types of meshes can be utilized at the interface:

- *Nodally equivalent meshes.* There is one-to-one correspondence between fluid and structure nodes at the interface.
- *Incompatible meshes.* This allows the use of separately designed meshes for fluid and structure and is more efficient (since structure meshes are normally coarser than fluid meshes). Data exchanges at the interface require least-squares projections.

The two solvers are loosely coupled in the current implementation, and the solution strategy proceeds as follows:

- Begin time step loop
  - Increment time step
  - Form predictors
  - Begin nonlinear loop
    - Transfer updated velocities and displacement to fluid
    - Solve mesh motion
    - Solve fluid component
    - Transfer updated pressures to structure
    - Solve structure component
  - End nonlinear loop
  - Form correctors
- End time step loop

5. MESH-MOVING SCHEME

In the case of the structural domain, the nodal displacements are computed as part of the solution process. For the fluid domain, the interior displacements due to motion at Γ_t^{fs} are obtained by using an automatic mesh-moving scheme [12], where the fluid mesh is modeled as a psuedo-linear elastic solid in static equilibrium.

6. PARALLEL IMPLEMENTATION

Both the fluid and structure solvers are implemented on distributed memory architectures using a message-passing paradigm. The parallel methodology within each solver is the same, here the meshes are partitioned into contiguous even-sized clusters of elements, and each cluster is mapped to a processor. Within each solver, a two-step communication route is set up between global and element data structures for the gather and scatter operations.

Communication between the solvers occurs through a master processor. The surface mesh at the interface is extracted from the fluid mesh and stored on the master processor along with the membrane component of the structure mesh (also lying on the interface). A communication trace is stored between the interface meshes and the associated solver. Data exchange at the interface is accomplished on the master processor and subsequently communicated to the other processors within the corresponding solver.

7. NUMERICAL EXAMPLE

In a preliminary application, we attempt to obtain the equilibrium shape of a ram-air parachute placed in a windstream. The structural mesh consists of 4,799 nodes, 9,454 two-noded cable elements, 4,796 four-noded membrane elements, and results in 13,356 equations. The fluid mesh consists of 247,437 nodes and 236,688 elements and results in 1,912,876 unknowns for fluid solver and 684,151 unknowns for mesh mover. The interface meshes are nodally equivalent. The lines in the parachute structure confluence at a fixed pivot point. The two sides of the parachute canopy

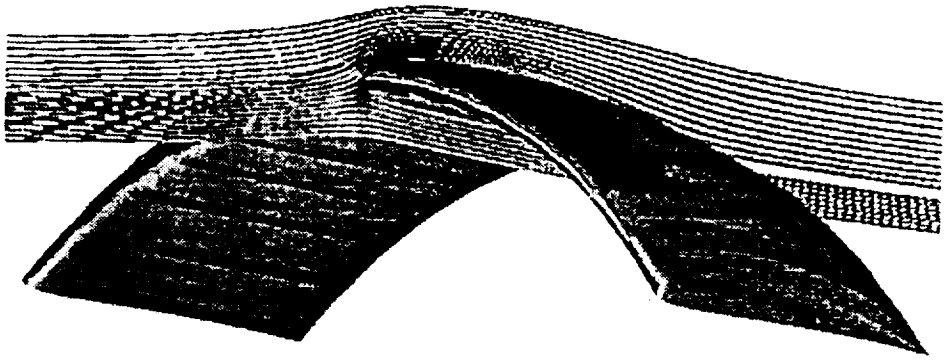

Figure 1. FSI application: parachute canopy in equilibrium configuration.

are constrained to move in the vertical plane. Since the flow within the canopy is not modeled, an internal pressure is imposed to represent the ram-air inflation. The parafoil ribs are modeled using cable elements and the lines are treated as slender cylinders to compute their contribution to the aerodynamic drag. The initial shape of the parafoil is assumed to be a smooth wing with $R/b = 0.6$ (where R is the radius of curvature and b is the span). Upon placement in the windstream and application of internal pressure, the parachute inflates to a 'bumby' shape and pitches back to a configuration where the moment due to line drag is balanced by the aerodynamic moment due to the canopy. Figure 1 shows the surface pressure on the parachute canopy together with stream tubes in the equilibrium configuration. This simulation was carried out on a CRAY T3E.

8. CONCLUDING REMARKS

We presented a methodology for parallel computation of 3D FSI problems. The methodology allows us to use compatible or incompatible interface meshes, adding a significant amount of flexibility. As a preliminary example, the method was applied to predict the equilibrium configuration of a ram-air parafoil placed in a wind stream.

9. ACKNOWLEDGMENT

This work was sponsored by NASA-JSC (grant NAG9-919), ARO (grant DAAH04-93-G-0514), and by the Army High Performance Computing Research Center under the auspices of the Department of the Army, Army Research Laboratory cooperative agreement number DAAH04-95-2-0003/contract number DAAH04-95-C-0008. The content does not necessarily reflect the position or the policy of the Government, and no official endorsement should be inferred. CRAY time was provided in part by the Minnesota Supercomputer Institute.

REFERENCES

[1] V. Kalro, S. Aliabadi, W. Garrard, T. Tezduyar, S. Mittal, and K. Stein, "Parallel finite element simulation of large ram-air parachutes", *International Journal for Numerical Methods in Fluids*, **24** (1997) 1353-1369.

[2] V. Kalro, W. Garrard and T.E. Tezduyar "Parallel finite element computation of the flare maneuver of a large ram-air parachute", *AIAA-97-1427, 14th Aerodynamic Decelerator Systems Conference*, San Francisco, (1997).

[3] R.J. Benney, K.R. Stein, J.W. Leonard and M.L. Accorsi, "Current 3-D structural dynamic finite element modeling capabilities", *AIAA-97-1506, Proceedings of the 14th Aerodynamic Decelerator Technology Conference*, San Francisco, 1997.

[4] K. Stein, R. Benney, V. Kalro, A. Johnson and T.E. Tezduyar "Parallel computation of parachute fluid-structure interactions", *AIAA-97-1505, 14th Aerodynamic Decelerator Systems Conference*, San Francisco, (1997).

[5] T.E. Tezduyar, M. Behr and J. Liou, "A new strategy for finite element computations involving moving boundaries and interfaces – the deforming-spatial-domain/space-time procedure: I. The concept and the preliminary tests", *Computer Methods in Applied Mechanics and Engineering*, **94** (1992) 339–351.

[6] T.E. Tezduyar, M. Behr, S. Mittal, and J. Liou, "A new strategy for finite element computations involving moving boundaries and interfaces – the deforming-spatial-domain/space-time procedure: II. Computation of free-surface flows, two-liquid flows, and flows with drifting cylinders", *Computer Methods in Applied Mechanics and Engineering*, **94** (1992) 353–371.

[7] T.J.R. Hughes and A.N. Brooks, "A multi-dimensional upwind scheme with no crosswind diffusion", in T.J.R. Hughes, editor, *Finite Element Methods for Convection Dominated Flows*, AMD-Vol.34, 19–35, ASME, New York, 1979.

[8] F. Brezzi and J. Pitkäranta,"On the stabilization of finite element approximations of the Stokes problem", in W. Hackbusch, editor, *Efficient Solutions of Elliptic Systems*, Notes on Numerical Fluid Mechanics-Vol.10, 11–19, Wiesbaden, 1984.

[9] K.J. Bathe, "Finite element procedures in engineering analysis", Prentice Hall Inc, New Jersey, 1982.

[10] A. Po,"Nonlinear dynamic analysis of cable and membrane structures", *Ph.D. Thesis*, Oregon State University, 1982.

[11] H.M. Hilber, T.J.R. Hughes and R.L. Taylor, "Improved numerical dissipation for time integration algorithms in structural dynamics", *Earthquake Engineering and Structural Dynamics*, **5** (1977) 283-292.

[12] A.A. Johnson and T.E. Tezduyar, "Mesh update strategies in parallel finite element computations of flow problems with moving boundaries and interfaces", *Computer Methods in Applied Mechanics and Engineering*, **119** (1994) 73–94.

Parachute Fluid-Structure Interactions: 3–D Computation

Keith Stein, [1] Richard Benney, [1] Vinay Kalro, [2] Tayfun Tezduyar, [2]
John Leonard, [3] and Michael Accorsi, [3]

1 U.S. Army Soldier Systems Command
Natick Research, Development and Engineering Center
Natick, Massachusetts, USA
kstein@natick-emh2.army.mil, rbenney@natick-emh2.army.mil
2 Aerospace Engineering and Mechanics, Army HPC Research Center
University of Minnesota, Minneapolis, Minnesota, USA
kalro@ahpcrc.umn.edu, tezduyar@ahpcrc.umn.edu
3 Department of Civil and Environmental Engineering
University of Connecticut, Storrs, Connecticut, USA
leonard@eng2.uconn.edu, accorsi@eng2.uconn.edu

1. INTRODUCTION

Parachute systems are deployed from a variety of aircraft in many different environments. These systems deploy a deceleration device, usually made of highly deformable fabrics, which must decelerate the payload to a survivable velocity before ground impact. Fluid-structure interactions (FSI) are involved at all stages of airdrop systems performance including at initial deployment, during inflation, at terminal descent (or gliding/maneuvering for steerable parachutes), and at soft landing (i.e., retraction for round parachutes, flared landing for ram-air parachutes). The interactions between the parachute system and the surrounding flow field are dominant in most parachute operations, and thus the ability to predict parachute fluid-structure interactions is of high interest to the Army [1,2].

The dynamics of parachutes are complex and difficult to model. They are governed by a highly nonlinear coupling between the structural dynamics of a highly deformable parachute system and the turbulent time-dependent flow field surrounding the parachute canopy. Advances in high-performance computing are making 3–D flow simulations and coupled fluid-structure computations for parachute problems more economical and feasible [3].

A strategy for performing 3–D parachute FSI simulations is being developed and initial results for application to a round parachute have been obtained. The FSI strategy will be broken into three components: the fluid dynamics (FD) solution, the structural dynamics (SD) solution, and the coupling of the FD and SD along the fluid-structure interface. The FD solution utilizes a stabilized space-time finite element formulation [4,5] of the time-dependent, 3–D Navier-Stokes equations with a zero-equation Smagorinsky turbulence model [6] to compute the flow fields. The problem is discretized with an unstructured finite element mesh to allow efficient meshing of the arbitrary spatial domains encountered [7]. For the SD solution, the equations of motion for the parachute system are solved using a finite element formulation for a "tension structure" composed of cables and membranes [8]. The

coupling of the FD with the SD is implemented over the fluid-structure interface, which is the parachute canopy surface. For FD and SD meshes with compatible sets of nodes defining the parachute surface, the coupling involves communication of necessary information between FD and SD surface nodes. For incompatible FD and SD meshes, coupling information must be computed with a more sophisticated projection algorithm [9]. To handle large deformations experienced in a parachute FSI, an automatic mesh moving scheme with occasional remeshing of the spatial domain is necessary [10]. This coupling approach has already been demonstrated on an axisymmetric parachute inflation simulation [11].

2. TEST PROBLEM: 3-D FSI FOR A ROUND PARACHUTE SYSTEM

A T–10 personnel parachute system is composed of a 35–foot diameter canopy and 30 29.4–foot suspension lines. The lines connect to two confluence points (which approximate the connection points for a personnel harness assembly). This system is allowed to inflate when the canopy is subjected to a differential pressure of 0.5 lb/ft^2. Figure 1 shows the SD model for the initial, nonstressed configuration of the parachute system, which has a flat extended skirt canopy with a vent at the apex and suspension lines that continue as 30 reinforcements through the parachute canopy. The parachute system is represented by linearly elastic materials, which have properties and dimensions representative of a T–10.

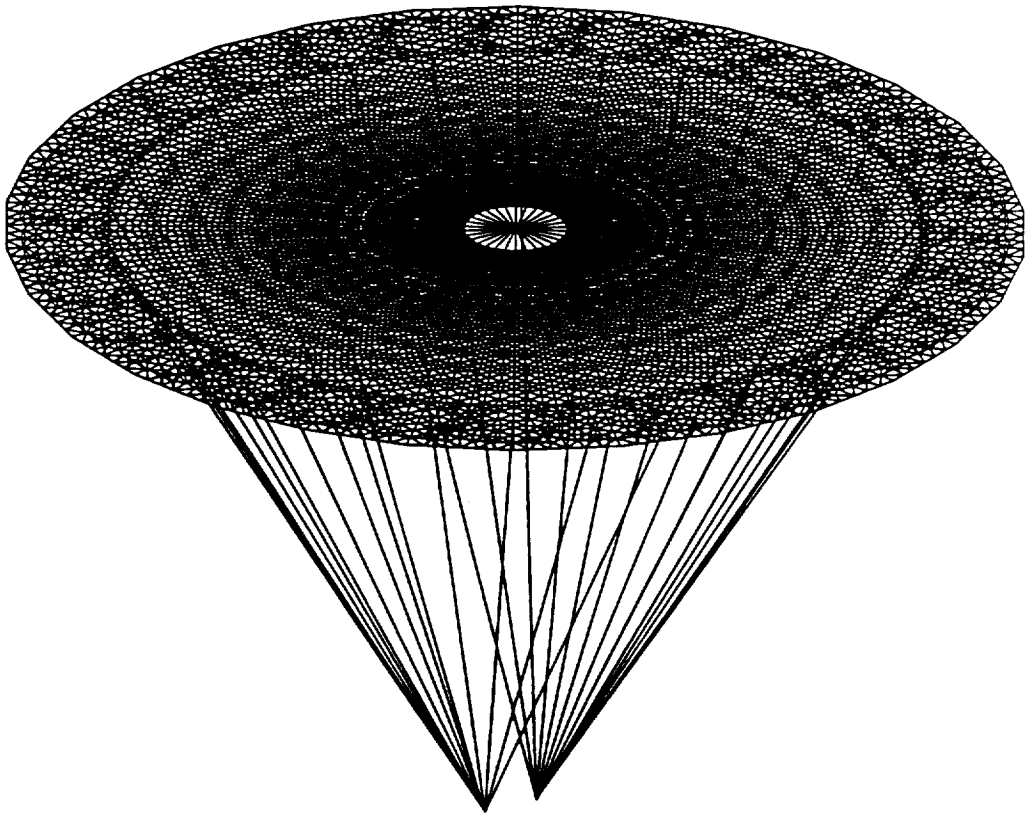

Figure 1. SD model in nonstressed configuration.

The SD model consists of 17,490 three–noded membrane elements and 1,920 two–noded cable elements for the suspension lines and canopy reinforcements. Figure 2 shows the fully inflated static configuration for the T–10 model under the prescribed pressure loading. Maximum principal stresses of the parachute canopy are superimposed on the surface, with low stresses along the canopy reinforcements and high stresses in the midgore regions.

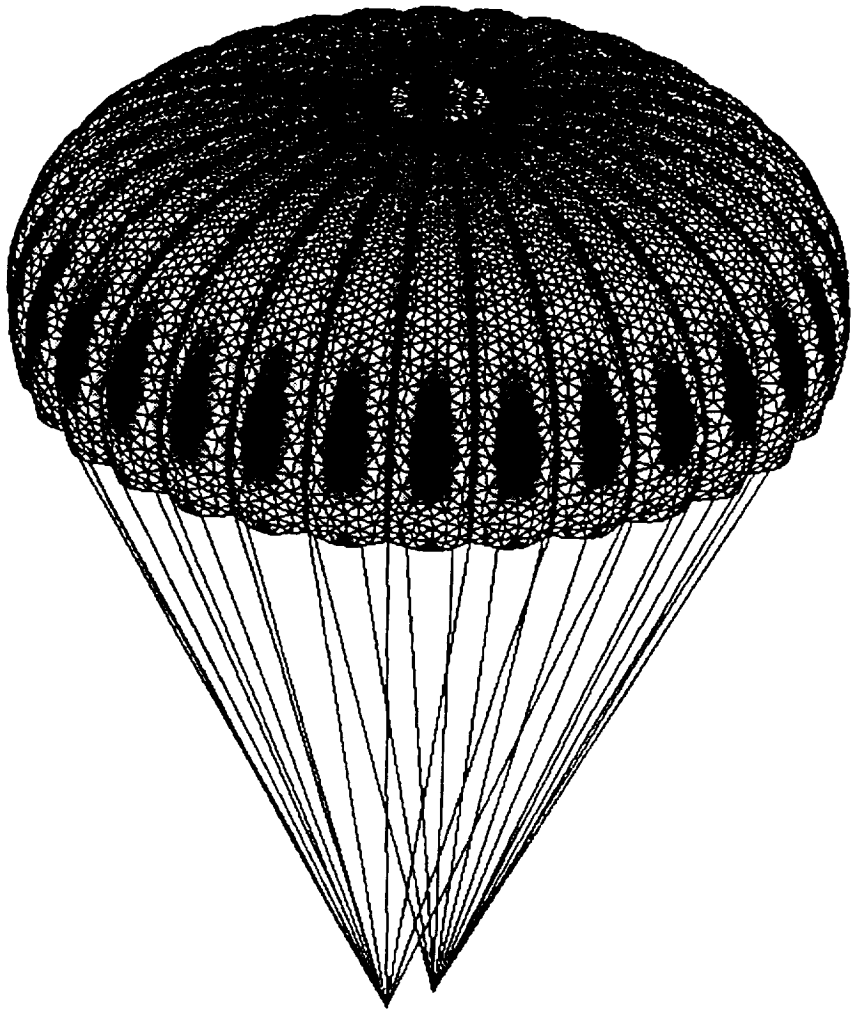

Figure 2. Fully inflated configuration for T–10 model.

A 3–D tetrahedral mesh was generated for the FD solution using the three–noded membrane mesh for the T–10 canopy in its inflated configuration as the surface mesh. Canopy surface nodes were multiply defined, with one node for both the upper and lower surface. Figure 3 shows the surface mesh for the canopy and a slice of the 3–D mesh bisecting the canopy. Initial unsteady flow solutions were obtained for flow about the fixed canopy configuration at a Reynolds number of 10^7 using a semi–discrete formulation of the incompressible Navier-Stokes equations. Figure 4 shows the computed velocities and pressures for the flow field about the T-10 canopy frozen at one instant in time. The FSI simulations are initiated using the stabilized space-

time formulation with the fully developed flow field for this configuration used as the initial condition.

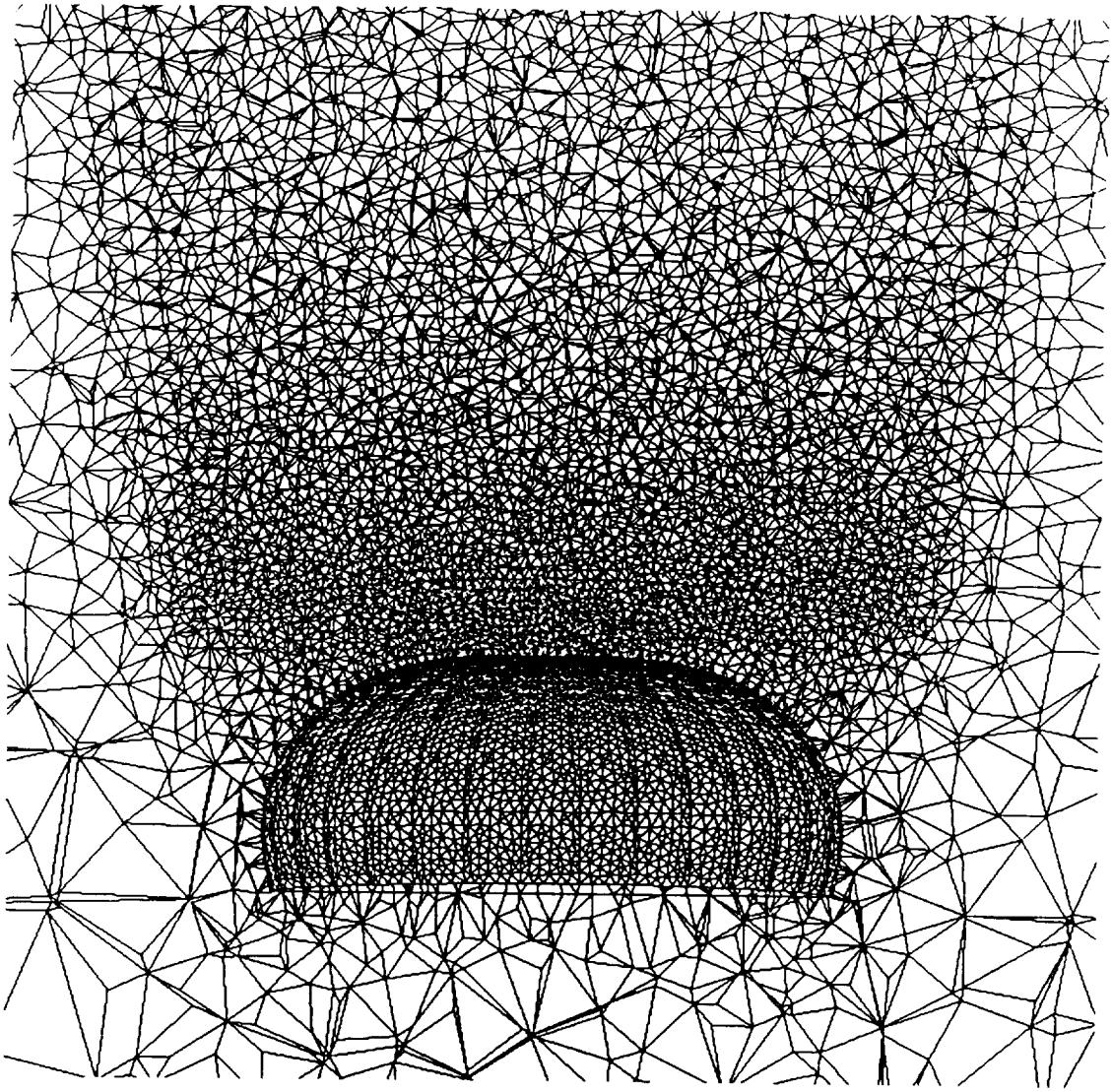

Figure 3. T–10 canopy surface mesh and slice of 3–D mesh bisecting canopy.

3. ACKNOWLEDGMENT

This work was sponsored by NASA–JSC (grant NAG9–919), ARO (grant DAAH04–93–G–0514), and by the Army High Performance Computing Research Center under the auspices of the Department of the Army, Army Research Laboratory cooperative agreement number DAAH04–95–2–0003/contract number DAAH04–95–C–0008. The content does not necessarily reflect the position or the policy of the Government, and no official endorsement should be inferred. CRAY time was provided in part by the Minnesota Supercomputer Institute.

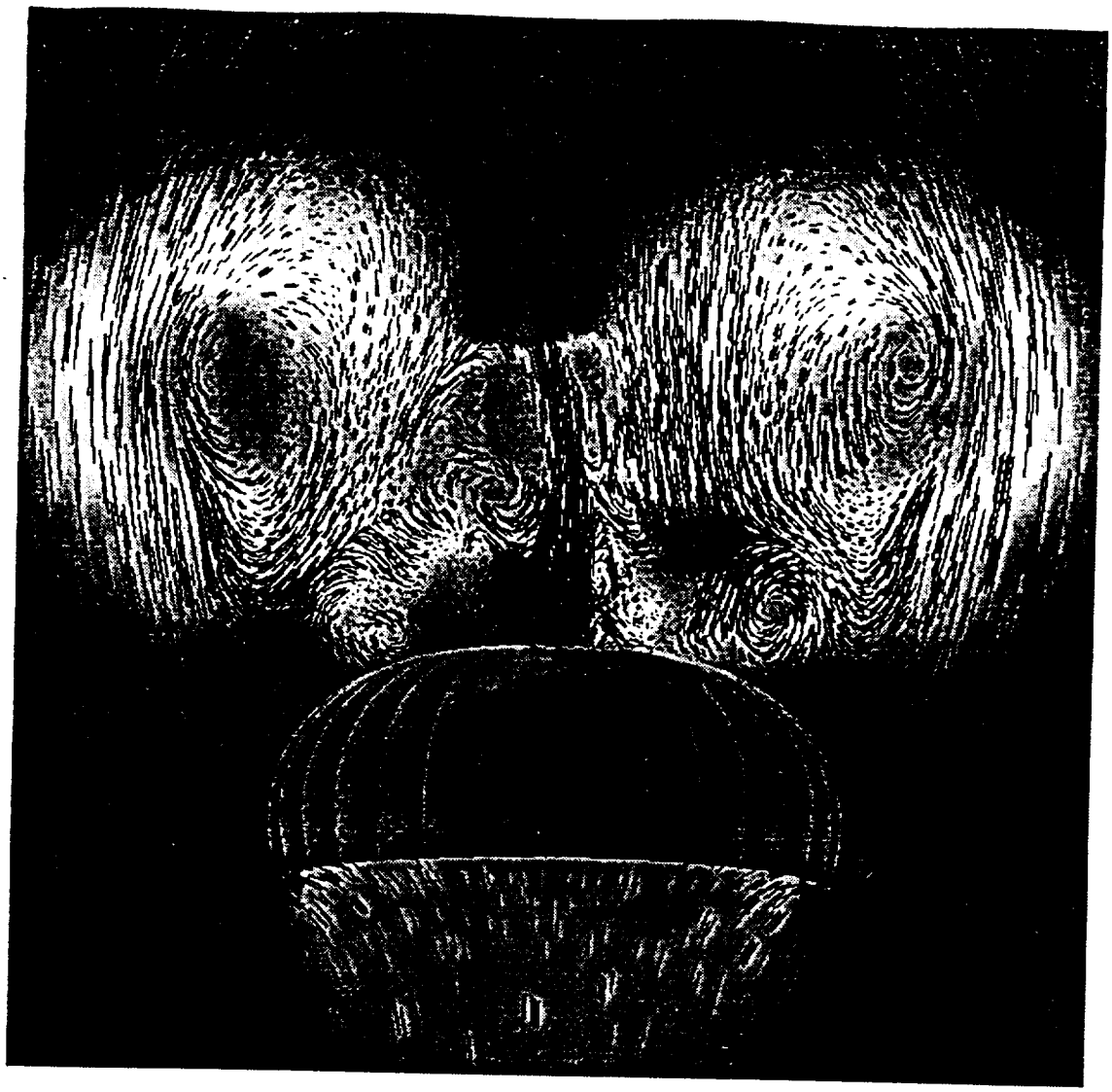

Figure 4. Computed flow field about T-10 model.

REFERENCES

[1] C.W. Peterson, J.H. Strickland and H. Higuchi, "The Fluid Dynamics of Parachute Inflation", *Annual Review of Fluid Mechanics*, **28** (1996) 361–387.

[2] R.J. Benney and K.R. Stein, "A Computational Fluid Structure Interaction Model for Parachute Inflation", *Journal of Aircraft*, **33** (1996) 730–736.

[3] V. Kalro, S. Aliabadi, W. Garrard, T. Tezduyar, S. Mittal and K. Stein, "Parallel Finite Element Simulation of Large Ram-Air Parachutes", *International Journal for Numerical Methods in Fluids*, **24** (1997) 1353–1369.

[4] T.E. Tezduyar, M. Behr and J. Liou, "A new strategy for finite element computations involving moving boundaries and interfaces - the deforming-spatial-domain/space-time procedure: I. The concept and the preliminary tests", *Computer Methods in Applied Mechanics and Engineering*, **94** (1992) 339–351.

[5] T.E. Tezduyar, M. Behr, S. Mittal and J. Liou, "A new strategy for finite element computations involving moving boundaries and interfaces - the deforming-spatial-domain/space-time procedure: II. Computation of free-surface flows, two-liquid flows, and flows with drifting cylinders", *Computer Methods in Applied Mechanics and Engineering*, **94** (1992) 353–371.

[6] J. Smagorinsky, "General Circulation Experiments with the Primitive Equations", *Monthly Weather Review*, **91** (1963) 99–165.

[7] A.A. Johnson and T.E. Tezduyar, "Parallel Computation of Incompressible Flows with Complex Geometries", *International Journal for Numerical Methods in Fluids*, **24** (1997) 1321–1340.

[8] R.J. Benney, K.R. Stein, J.W. Leonard and M.L. Accorsi, "Current 3-D Structural Dynamic Finite Element Modeling Capabilities", *Proceedings of the 14th AIAA Aerodynamic Decelerator Technology Conference*, San Francisco, 1997.

[9] N. Maman and C. Farhat, "Matching Fluid and Structure Meshes for Aeroelastic Computations: A Parallel Approach", *Computers and Structures*, **54** (1995) 779–785.

[10] A.A. Johnson and T.E. Tezduyar, "Mesh Update Strategies in Parallel Finite Element Computations of Flow Problems with Moving Boundaries", *Computer Methods in Applied Mechanics and Engineering*, **119** (1994) 73–94.

[11] K.R. Stein, R.J. Benney, V. Kalro, A.A. Johnson and T.E. Tezduyar, "Parallel Computation of Parachute Fluid–Structure Interactions", *Proceedings of the 14th AIAA Aerodynamic Decelerator Technology Conference*, San Francisco, 1997.

MULTI-DOMAIN PARALLEL COMPUTATION OF WAKE FLOWS AROUND SECONDARY OBJECTS

Yasuo Osawa [1], Vinay Kalro [1] and Tayfun Tezduyar [1]

[1] Army High Performance Computing Research Center,
1100 Washington Ave. South, Minneapolis, MN, 55415, USA
osawa@ahpcrc.umn.edu
kalro@ahpcrc.umn.edu
tezduyar@ahpcrc.umn.edu

1. INTRODUCTION

With the recent advances in flow simulation and modeling methods and the advanced parallel supercomputers, we now have powerful computational tools capable of simulating complex flow problems in applied fluid mechanics. Methods designed for a general class of challenging flow problems sometimes need to be re-designed and/or optimized for more specific classes of problems which pose their own specific challenges. One of these specific classes of problems is 3D simulation of unsteady wake flow generated by a primary (leading) object and how the wake flow affects a secondary (trailing) object placed in this wake. Examples of this class of applications are flow around a small aircraft in the wake of a larger aircraft, and flow around a parachute crossing the wake flow of an aircraft. In many cases, because the two objects are separated by a large distance compared to the length scales of the objects, these wake regions are rather long, and we need to take this fact into account in developing computational methods which will be effective for this particular class of problems.

In this paper, we present a multi-domain parallel computational method for simulation of unsteady flow past the primary object, unsteady wake flow in the long region between the two objects, and the influence of this wake flow on the secondary object. The base method is a finite element formulation with the streamline-upwind/Petrov-Galerkin (SUPG) [1] and pressure-stabilizing/Petrov-Galerkin (PSPG) [2] stabilizations. With these stabilization techniques, simulations can be carried out for flows with high Reynolds numbers and thin boundary layers, without generating numerical oscillations but also without introducing excessive numerical dissipation to the computations. Furthermore, these stabilization techniques allow us to use equal-order interpolation functions (such as trilinear-trilinear and linear-linear) for velocity and pressure without generating any numerical oscillations that would normally be caused by such combinations of interpolation functions.

The spatial discretization of the finite element formulation leads to a set of coupled, nonlinear, ordinary differential equations which are solved with a predictor/multi-corrector time marching scheme. At each time step, a set of coupled, nonlinear equations is solved with the Newton-Raphson iterations. At each Newton-Raphson iteration, a set of coupled, linear equations is solved with iterative methods with the GMRES [3] update technique. In computation of vector-matrix products involved in

this innermost iterations, we have been using element-matrix-based, element-vector-based (also called matrix-free) [4], and sparse-matrix-based [5] methods. These methods, particularly the last two, can be very effectively used for simulation of problems with millions of equations. The overall formulation and the solution techniques have been implemented on parallel computing platforms by using the MPI programming environment. The parallel platforms used include CRAY T3D, CRAY T3E and the SGI POWER CHALLENGE with the R8000 processor.

The multi-domain computation approach is based on dividing the entire simulation domain into an ordered sequence of overlapping subdomains. The flow field computed over a leading subdomain is used in specifying the inflow boundary conditions for the following subdomain. The inflow conditions for the first subdomain are extracted from the free-stream conditions. Subdomain-1 is used for computation of the unsteady flow around the primary object. Because the primary object typically would have a complex geometry, such as an aircraft geometry, the mesh constructed over Subdomain-1 would typically be an unstructured one. Therefore, the computation over Subdomain-1 would require a general-purpose finite element implementation. Subdomain-2 would be used for computation of the unsteady wake flow generated by the primary object, and this subdomain would typically be much longer compared to Subdomain-1. Since Subdomain-2 would not involve any objects, the mesh constructed over this domain could be a structured mesh, perhaps even a uniform one. A special-purpose finite element implementation recognizing the uniform nature of the mesh can be optimized to yield much higher computational speeds compared to a general-purpose implementation. In fact, the computation over Subdomain-2 can be accomplished by methods other than the finite element method, such as the spectral method, that might be more desirable for computations over very regular geometries. The computation over Subdomain-3, which would contain the secondary object, would typically require, similar to Subdomain-1, an unstructured mesh, and consequently a general-purpose finite element implementation. We also note that computations over these different subdomains can be performed on different computing platforms and almost in parallel, provided a leading subdomain is at least one time step ahead of the following subdomain.

We need to place the inflow boundary of Subdomain-2 sufficiently ahead of the outflow boundary of Subdomain-1, so that the input to Subdomain-2 is sufficiently clear of any truncation effects at the downstream boundary of Subdomain-1. Furthermore, this input needs to be captured early enough before the solution in Subdomain-1 enters the coarser regions of the mesh towards the downstream boundary. Similarly, the inflow boundary of Subdomain-3 needs to be placed sufficiently ahead of the outflow boundary of Subdomain-2, which in turn needs to be sufficiently distant from the secondary object.

To demonstrate this multi-domain approach, we computed flow problems involving cylinders and wing-shaped objects. In the case of flow past a cylinder, our purpose was to verify the validity of some of the concepts used and to capture vortex shedding in wake regions very far from the cylinder. Due to space limitations, we will not be presenting these results in this paper. In the next section, we present the computation with three subdomains, where the first and last subdomains include wing-shaped objects.

2. NUMERICAL EXAMPLE: WING-SHAPED PRIMARY AND SECONDARY OBJECTS

In this 3D simulation, we compute on SGI POWER CHALLENGE and CRAY T3E unsteady flow past a leading large wing and two trailing small wings placed in the far wake of the larger one and affected by its wing tip vortices (see Figure 1). The Reynolds number is 1000 for the leading wing. We assume symmetry with respect to the plane passing through the middle of the primary wing and the two trailing ones. Subdomain-1 contains half of the primary wing and is handled with a general-purpose finite element implementation (see Figure 1). Subdomain-2 is the wake region and is handled with a special-purpose implementation and a structured mesh. Subdomain-3 contains one of the trailing wings and is handled with a general-purpose implementation and an unstructured mesh[1] (see Figure 2). The leading and trailing wings both have rectangular shapes, an aspect ratio of 8, NACA0012 cross-section, and an angle of attack of 8.0 degrees. The trailing wing has half the cord-length of the leading wing.

Figure 3 shows the results for the leading wing and the wake region. The results for the trailing wing are shown in Figure 4. For the leading wing, we see the tip vortices as well as a vortex shedding that quickly dissipates downstream because of the coarse mesh. For the wake region, we see the wing tip vortices and the vortex shedding. Figure 4 (Left) shows, for the trailing wing, the vertical component of the velocity at three vertical planes: the right wing tip, the center, and the left wing tip. The left wing tip has more exposure to the wing tip vortices from the leading wing. Figure 4 (Right) shows the rolling moment for the trailing wing, compared to the case when that wing is in a uniform flow field.

3. ACKNOWLEDGMENT

This work was supported by the ARO (grant DAAH04-93-G-0514), NASA (grant NAG9-919), and by the Army High Performance Computing Research Center under the auspices of the Department of the Army, Army Research Laboratory cooperative agreement number DAAH04-95-2-0003/contract number DAAH04-95-C-0008. The content does not necessarily reflect the position or the policy of the Government, and no official endorsement should be inferred. CRAY time was provided in part by the Minnesota Supercomputer Institute. The first author has been supported by the Bridgestone Corp.

[1]The mesh generator was developed by the Team for Advanced Flow Simulation and Modeling (T*AFSM) at the Army HPC Research Center.

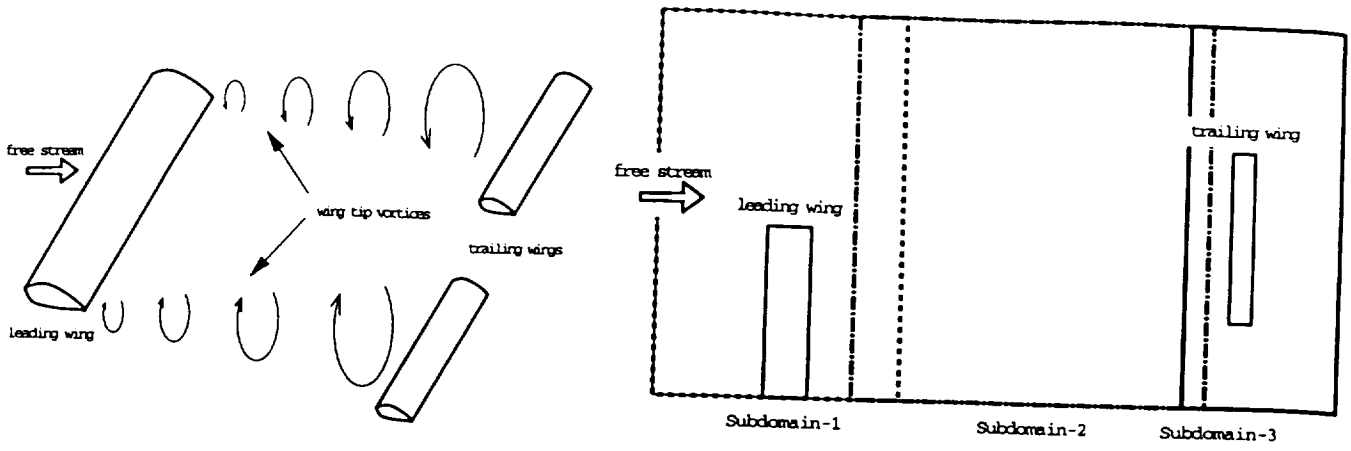

Figure 1. Arrangement of the wings and the subdomains.

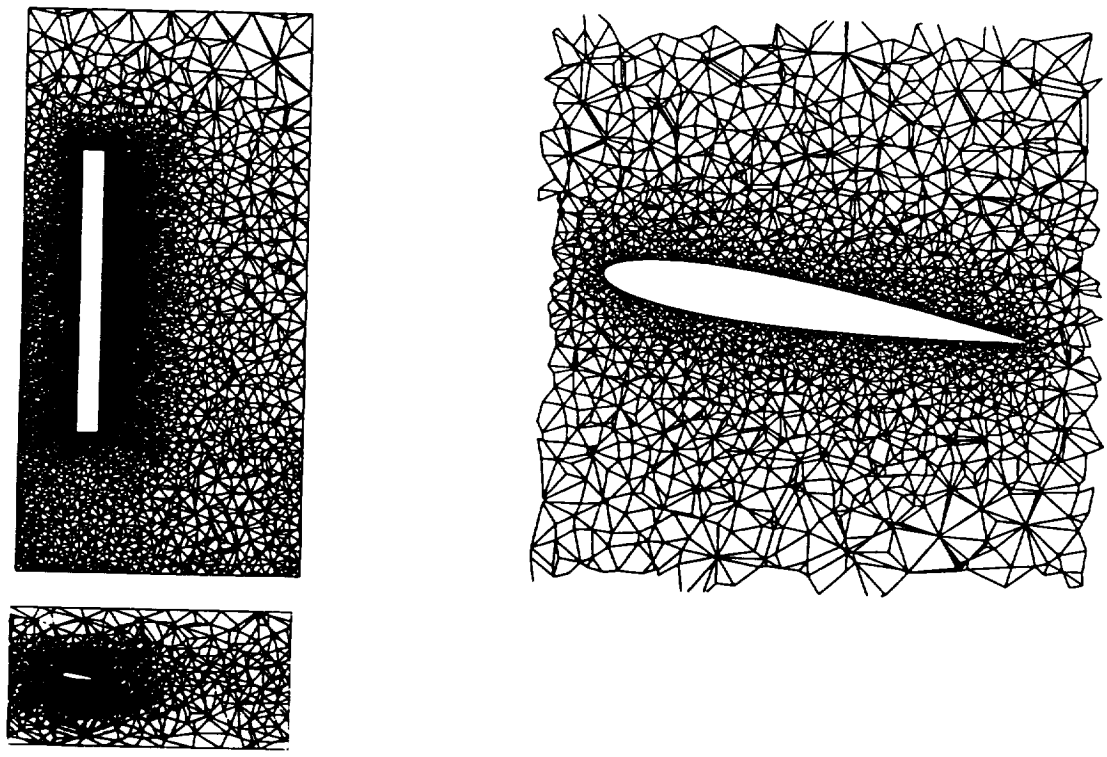

Figure 2. Unstructured mesh for the trailing wing

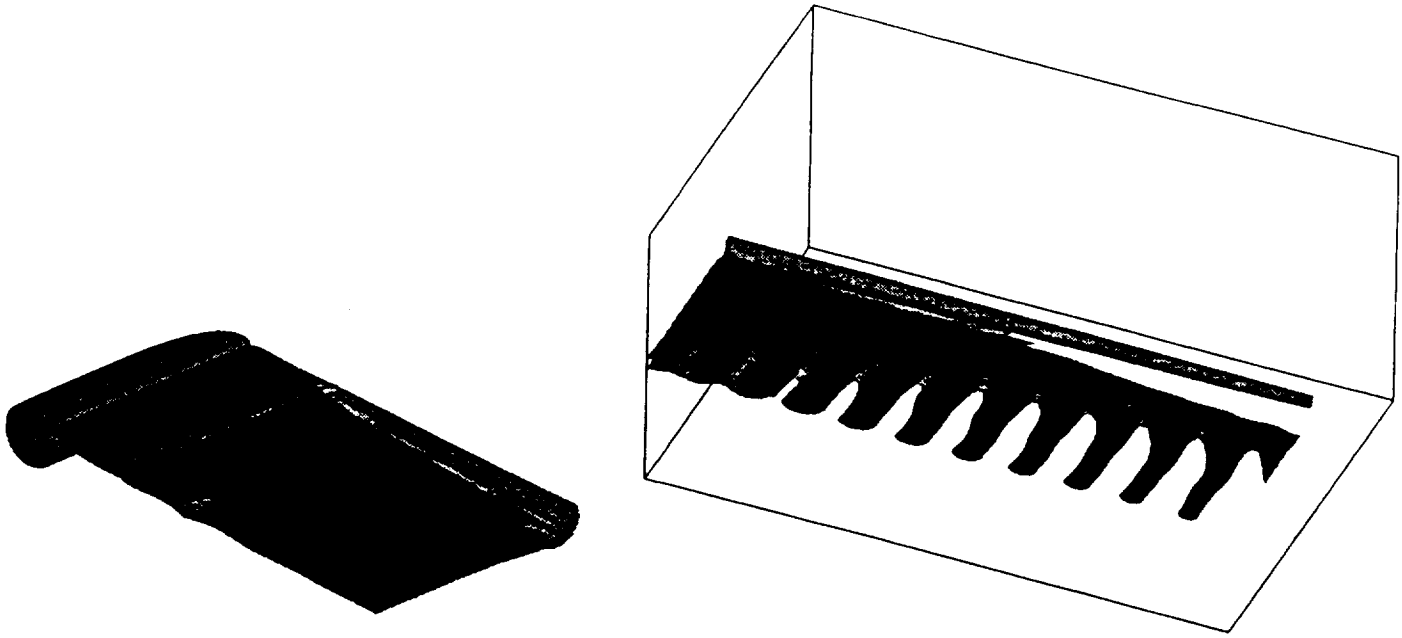

Figure 3. Iso-surfaces for the leading wing (left) and the wake region (right). Left: streamwise component of the velocity (corresponding to 97.5% of the free-stream value). Right: spanwise and streamwise components of the vorticity (corresponding to .5 value).

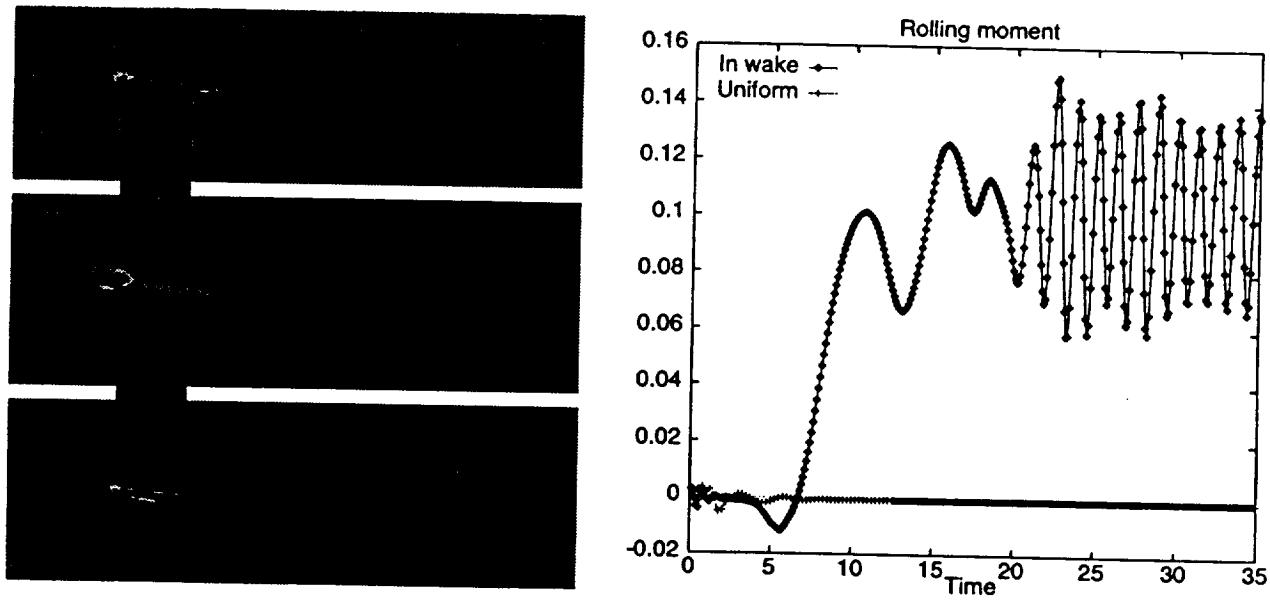

Figure 4. Left: vertical component of the velocity at three vertical planes: the right wing tip, the center, and the left wing tip. Right: rolling moment for the trailing wing, compared to the case when that wing is in a uniform flow field.

[1] A.N. Brooks and T.J.R. Hughes, "Streamline upwind/Petrov-Galerkin formulations for convection dominated flows with particular emphasis on the incompressible Navier-Stokes equations", *Computer Methods in Applied Mechanics and Engineering*, **32** (1982) 199–259.

[2] T.E. Tezduyar, "Stabilized finite element formulations for incompressible flow computations", *Advances in Applied Mechanics*, **28** (1991) 1–44.

[3] Y. Saad and M. Schultz, "GMRES: A generalized minimal residual algorithm for solving nonsymmetric linear systems", *SIAM Journal of Scientific and Statistical Computing*, **7** (1986) 856–869.

[4] Z. Johan, T.J.R. Hughes, and F. Shakib, "A globally convergent matrix-free algorithm for implicit time-marching schemes arising in finite element analysis in fluids", *Computer Methods in Applied Mechanics and Engineering*, **87** (1991) 281–304.

[5] V. Kalro and T. Tezduyar, "Parallel iterative computational methods for 3d finite element flow simulations", to appear in *Computer Assisted Mechanics and Engineering Sciences*, 1997.

A MULTI-DOMAIN METHOD FOR COMPUTATION OF LONG-WAKE FLOWS

Yasuo Osawa, Vinay Kalro and Tayfun Tezduyar

Mechanical Engineering and Materials Science
Army High Performance Computing Research Center
Rice University - MS 321, 6100 Main Street
Houston, TX 77005-1892, USA

SUMMARY

We present a multi-domain computational method for simulation of unsteady flow past a primary object, unsteady wake flow in the long region behind the primary object, and the influence of this wake flow on a secondary object. The multi-domain computation approach is based on dividing the entire simulation domain into an ordered sequence of overlapping subdomains. The flow field computed over a leading subdomain is used in specifying the inflow boundary conditions for the following subdomain. Over subdomains which do not involve any complex-shaped objects, we use special-purpose implementation of our flow solver to carry out the computation more efficiently. To demonstrate the potential and power of this multi-domain approach, we present 3D computational results for flow problems involving cylinders and wing-shaped objects.

INTRODUCTION

Advanced methods we have developed in recent years for flow simulation and modeling and the modern parallel supercomputers gave us powerful computational tools capable of simulating complex flow problems in many challenging fluid mechanics applications. However, methods designed for a general class of challenging flow problems sometimes need to be redesigned and/or optimized to more effectively address specific classes of problems which pose their own specific challenges. One of such specific classes of problems is 3D simulation of unsteady wake flow generated by a primary (leading) object and how the wake flow affects a secondary (trailing) object placed at a distant location in this wake. Examples of this class of applications are flow around a small aircraft in the wake of a larger aircraft, and flow around a parachute crossing the wake flow of an aircraft. In many such cases, because the two objects are separated by a large distance compared to the length scales of the objects, these wake regions have to be relatively long. Consequently, we need to take this requirement into account in developing computational methods which will be effective for this particular class of problems.

The multi-domain computational method described in this paper was developed for this purpose. With this method, we can compute, with two level of parallelism, unsteady flow past the primary object, unsteady wake flow in the long region between the two objects, and the influence of this wake flow on the secondary object. We start with a stabilized finite element formulation with the streamline-upwind/Petrov-Galerkin (SUPG) [1] and pressure-stabilizing/Petrov-Galerkin (PSPG) [2] stabilizations. With these stabilization techniques, simulations can be carried out for flows with high Reynolds numbers and thin boundary layers, without generating numerical oscillations but also without introducing excessive numerical dissipation to the computations. Furthermore, these stabilization techniques allow us to use equal-order interpolation functions (such as trilinear-trilinear and linear-linear) for velocity and pressure without generating any numerical oscillations that would normally be caused by such combinations of interpolation functions.

The spatial discretization of the finite element formulation leads to a set of coupled, nonlinear, ordinary differential equations which are solved with a predictor/multi-corrector time marching scheme. At each time step, a set of coupled, nonlinear equations is solved with the Newton-Raphson iterations. At each Newton-Raphson iteration, a set of coupled, linear equations is solved with iterative methods with the GMRES [3] update technique. In computation of vector-matrix products involved in this innermost iterations, we have been using element-matrix-based, element-vector-based (also called matrix-free) [4], and sparse-matrix-based [5] methods. These methods, particularly the last two, can be very effectively used for simulation of problems with millions of equations. The overall formulation and the solution techniques have been implemented on parallel computing platforms by using the MPI programming environment. The parallel platforms used include CRAY T3D, CRAY T3E and the SGI POWER CHALLENGE with the R8000 processor.

In the multi-domain computation approach, we divide the full simulation domain into an ordered sequence of slightly overlapping subdomains. The in-

flow boundary conditions for a subdomain is extracted from the the flow field computed over the preceding subdomain. The inflow conditions for the first subdomain are extracted from the free-stream conditions. Subdomain-1 is used for computation of the unsteady flow around the primary object. Because the primary object typically would have a complex geometry, such as an aircraft geometry, the mesh constructed over Subdomain-1 would typically be an unstructured one. Therefore, the computation over Subdomain-1 would require a general-purpose finite element implementation. Subdomain-2 would be used for computation of the unsteady wake flow generated by the primary object, and this subdomain would typically be much longer compared to Subdomain-1. Since Subdomain-2 would not involve any objects, the mesh constructed over this domain could be a structured mesh, perhaps even a uniform one. A special-purpose finite element implementation recognizing the uniform nature of the mesh can be optimized to yield much higher computational speeds compared to a general-purpose implementation. In fact, the computation over Subdomain-2 can be accomplished by methods other than the finite element method, such as the spectral method, that might be more desirable for computations over very regular geometries. The computation over Subdomain-3, which would contain the secondary object, would typically require, similar to Subdomain-1, an unstructured mesh, and consequently a general-purpose finite element implementation. We also note that while for each subdomain the computation is carried out in parallel, a second level of inherent parallelism can be exploited by recognizing that computations over these different subdomains can be performed on different computing platforms and almost in parallel, provided a leading subdomain is at least one time step ahead of the following subdomain.

We need to place the inflow boundary of Subdomain-2 sufficiently ahead of the outflow boundary of Subdomain-1, so that the input to Subdomain-2 is sufficiently clear of any truncation effects at the downstream boundary of Subdomain-1. Furthermore, this input needs to be captured early enough before the solution in Subdomain-1 enters the coarser regions of the mesh towards the downstream boundary. Similarly, the inflow boundary of Subdomain-3 needs to be placed sufficiently ahead of the outflow boundary of Subdomain-2, which in turn needs to be sufficiently distant from the secondary object.

To demonstrate this multi-domain approach, we computed flow problems involving cylinders and wing-shaped objects. In the case of flow past a cylinder, our purpose was to verify the validity of some of the concepts used and to capture vortex shedding in wake regions very far from the cylinder. In the case of flow past wings in tandem, we compute flow past a leading wing in Subdomain-1, in the long-wake region (Subdomain-2), and the effect of this wake flow on a trailing wing in Subdomain-3.

NUMERICAL RESULTS

Cylinder Wake Computation at $Re = 300$ with a Highly Refined Mesh

We compute the unsteady flow past a circular cylinder to compare the single- and the multi-domain methods. The single-domain computation uses the same mesh as Kalro and Tezduyar [6], and the multi-domain computation uses a highly refined mesh (see Figure 1).

Compared to the single-domain model, the number of element in the wake domain is ~3.3 times larger in the streamwise direction, ~1.8 times larger in the crossflow direction, and 2.0 times larger in the spanwise direction.

Figure 2 shows vorticity iso-surface for these computations. Figure 3 shows the streamwise component of vorticity at the centered horizontal plane.

These figures clearly show that the solution for the multi-domain computation catch greater details of flow features, and these features are maintained all the way to the outflow boundary.

Cylinder Long-Wake Computation at $Re = 140$

The second phase vortex shedding in the far wake of a cylinder was first reported by Taneda [7], followed by many other researchers [8-11]. The second phase shedding is reported at Re=140, which is within laminar regime. Cimbala [9] attributes this phenomena to hydrodynamic instability, while Williamson [11] suggested that this is caused by the sensitivity of the wake to small-scale perturbations. 3D numerical simulation of this problem is not an easy task because of the long domain required ($300\bar{d}$). This motivated us to simulate it using a multi-domain computation.

First a 2D simulation was performed. The entire domain was divided into two subdomains: one around the cylinder, and the other one in the wake domain, starting at $2\bar{d}$ downstream from the center of the cylinder until $300\bar{d}$, with one element in spanwise direction (see Figure 4). The wake domain model consists of 1,824,066 nodes and 905,920 hexahedral elements, resulting in 5,446,832 nonlinear equations.

Figure 5 shows the magnitude of vorticity in the wake subdomain. No second phase vortex shedding is observed in the far wake, though the Karman vortex street is captured in the near wake. From laboratory experiments, the transition between these two phases is expected at $100\sim150\bar{d}$. However in our simulation, vorticity decays in that region (see Figure 5). This leads us to believe that the 3D effects are the cause of the second phase vortex shedding.

A 3D model is considered as the second computation for the same problem with three subdomains: one around the cylinder; another in the first wake subdomain, starting at $2\bar{d}$ downstream from the center of the cylinder until $155\bar{d}$ to catch transition; followed by second wake subdomain starting at $150\bar{d}$ until $300\bar{d}$. Each wake subdomain model has more than four million nodes and hexahedral elements, and results in more than 17 million nonlinear equations. The computation over each wake subdomain requires, for each time step, about 36 seconds on 128 processors of the CRAY T3E-1200. Figure 6 shows the magnitude of vorticity at horizontal center plane in both subdomains.

The first wake subdomain captures the transition of vortex shedding near outflow boundary, and the second one successfully captures the second phase vortex shedding. The spacing between the vortices in the second phase vortex shedding is about twice as large compared to the spacing we see in the first phase. Figure 7 shows the streamwise component of the vorticity in the first wake subdomain.

Figure 7 shows the existence of streamwise vortices which are similar to the those seen at Re=300. The streamwise vortices interact with the spanwise vortices and break down the first phase vortex shedding. From these results, we observe that the existence of streamwise vortices, which is a 3D behavior. These vortices make the first phase vortex shedding transform to the second phase vortex shedding at Re=140.

Flow Past Wings in Tandem

In this 3D simulation, we compute on SGI POWER CHALLENGE and CRAY T3E unsteady flow past a leading large wing and two trailing small wings placed in the far wake of the larger one and affected by its wing tip vortices (see Figure 8). The Reynolds number is 1000 for the leading wing. We assume symmetry with respect to the plane passing through the middle of the primary wing and the two trailing ones. Subdomain-1 contains half of the primary wing and is handled with a general-purpose finite element implementation (see Figure 8). Subdomain-2 is the wake region and is handled with a special-purpose implementation and a structured mesh. Subdomain-3 contains one of the trailing wings and is handled with a general-purpose implementation and an unstructured mesh[1] (see Figure 9). The leading and trailing wings both have rectangular shapes, an aspect ratio of 8, NACA0012 cross-section, and an angle of attack of 8.0 degrees. The trailing wing has half the cord-length of the leading wing.

Figure 10 shows the results for the leading wing and the wake region. The results for the trailing wing are shown in Figure 11. For the leading wing, we see the tip vortices as well as a vortex shedding that quickly dissipates downstream because of the coarse mesh. For the wake region, we see the wing tip vortices and the vortex shedding. Figure 11 (left) shows, for the trailing wing, the vertical component of the velocity at three vertical planes: the right wing tip, the center, and the left wing tip. The left wing tip has more exposure to the wing tip vortices from the leading wing. Figure 11 (right) shows the rolling moment for the trailing wing, compared to the case when that wing is in a uniform flow field.

[1]The mesh generator was developed by the Team for Advanced Flow Simulation and Modeling (T*AFSM) at the Army HPC Research Center.

ACKNOWLEDGMENT

This work was supported by the ARO (grant DAAH04-93-G-0514), NASA (grant NAG9-919), and by the Army High Performance Computing Research Center under the auspices of the Department of the Army, Army Research Laboratory cooperative agreement number DAAH04-95-2-0003/contract number DAAH04-95-C-0008. The content does not necessarily reflect the position or the policy of the Government, and no official endorsement should be inferred. The first author has been supported by the Bridgestone Corp.

REFERENCES

1. A.N. Brooks and T.J.R. Hughes, "Streamline upwind/Petrov-Galerkin formulations for convection dominated flows with particular emphasis on the incompressible Navier-Stokes equations", *Computer Methods in Applied Mechanics and Engineering*, **32** (1982) 199–259.

2. T.E. Tezduyar, "Stabilized finite element formulations for incompressible flow computations", *Advances in Applied Mechanics*, **28** (1991) 1–44.

3. Y. Saad and M. Schultz, "GMRES: A generalized minimal residual algorithm for solving nonsymmetric linear systems", *SIAM Journal of Scientific and Statistical Computing*, **7** (1986) 856–869.

4. Z. Johan, T.J.R. Hughes, and F. Shakib, "A globally convergent matrix-free algorithm for implicit time-marching schemes arising in finite element analysis in fluids", *Computer Methods in Applied Mechanics and Engineering*, **87** (1991) 281–304.

5. V. Kalro and T. Tezduyar, "Parallel iterative computational methods for 3d finite element flow simulations", to appear in *Computer Assisted Mechanics and Engineering Sciences*, 1997.

6. V. Kalro and T.E. Tezduyar, "Parallel 3d computation of unsteady flows around circular cylinder", *Parallel Computing*, **23** (1997) 1235–1248.

7. S. Taneda, "Downstream development of the wakes behind cylinder", *Journal of the physical society of Japan*, **14** (1959) 843–848.

8. T. Matsui and M. Okude, "Formation of the secondary vortex street in the wake of a circular cylinder", in *Structure of complex turbulent shear flow*, (1983) 156–164.

9. J.M. Cimbala, H.M. Nagib, and A. Roshko, "Large structure in the far wakes of two-dimensional bluff bodies", *Journal of Fluid Mechanics*, **190** (1988) 265–298.

10. O. Inoue, T. Yamazaki, and T. Bisaka, "Numerical simulation of forced wakes around a cylinder", *International Journal heat and fluid flow*, **16** (1995) 327–332.

11. C.H.K. Williamson, "Vortex dynamics in the cylinder wake.", *Annual Review of Fluid Mechanics*, **28** (1996) 477–539.

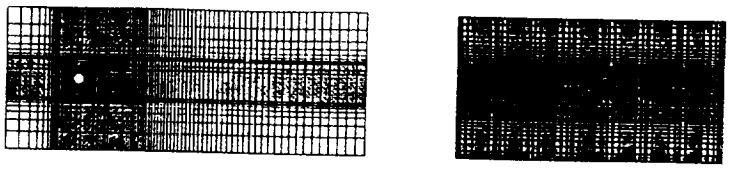

Figure 1. Cylinder wake computation at $Re = 300$ with a highly-refined mesh. Mesh for the single-domain computation (left) and for the multi-domain computation (right).

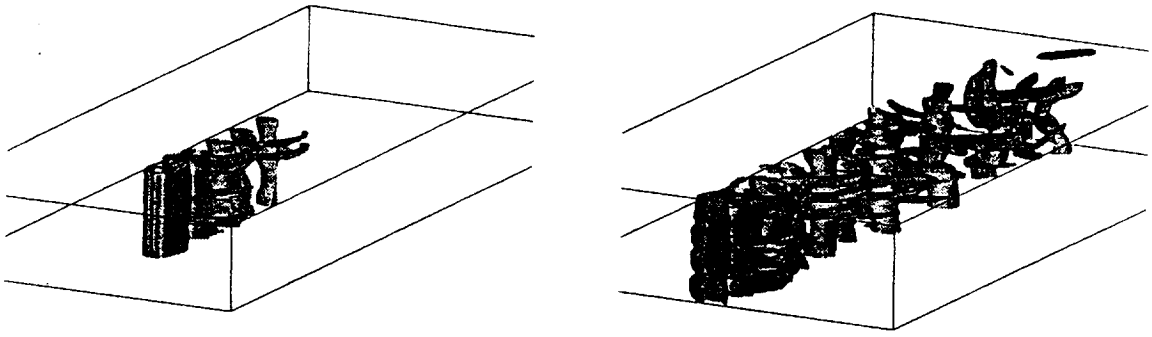

Figure 2. Cylinder wake computation at $Re = 300$ with a highly-refined mesh. Vorticity iso-surfaces corresponding to 0.6 value, obtained with the single-domain computation (left) and the multi-domain computation (right).

Figure 3. Cylinder wake computation at $Re = 300$ with a highly-refined mesh. The streamwise component of vorticity at the centered horizontal plane, obtained with the single-domain computation (left) and the multi-domain computation (right).

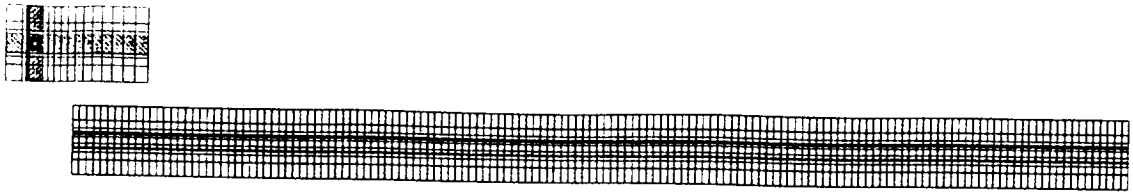

Figure 4. 2D cylinder long-wake computation at $Re = 140$. Arrangement of the two subdomains. Frames do not show the actual mesh.

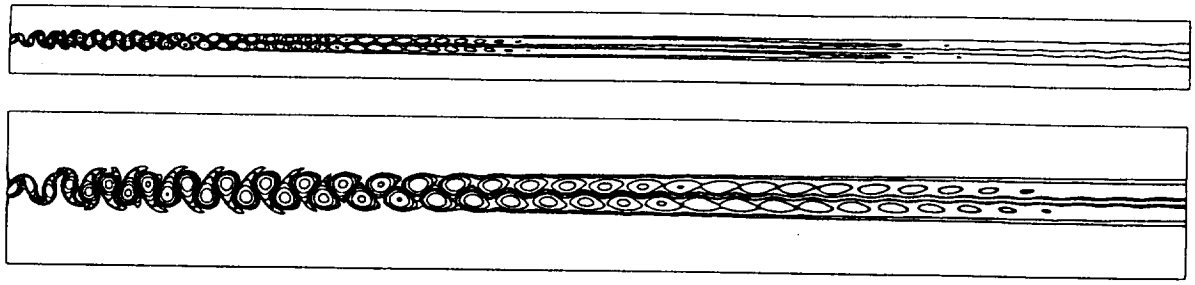

Figure 5. 2D cylinder long-wake computation at $Re = 140$. Magnitude of the vorticity for the entire Subdomain-2 (upper) and upstream half of Subdomain-2 (lower).

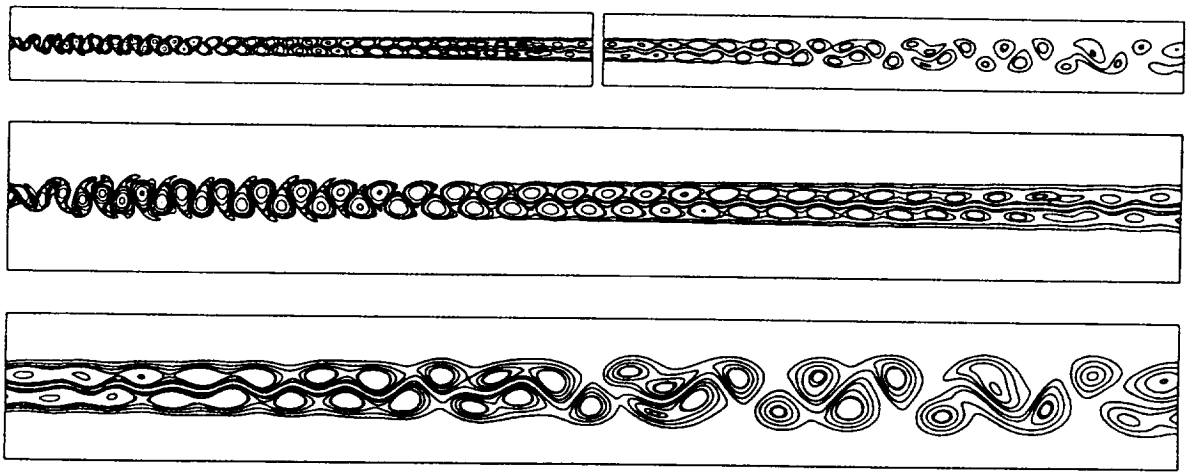

Figure 6. 3D cylinder long-wake computation at $Re = 140$. Magnitude of the vorticity for Subdomain-2 and Subdomain-3 (upper left and right), Subdomain-2 (middle), and Subdomain-3 (with smaller magnitude of contours) (lower).

Figure 7. 3D cylinder long-wake computation at $Re = 140$. Streamwise component of the vorticity at the centered horizontal plane, shown for Subdomain-2.

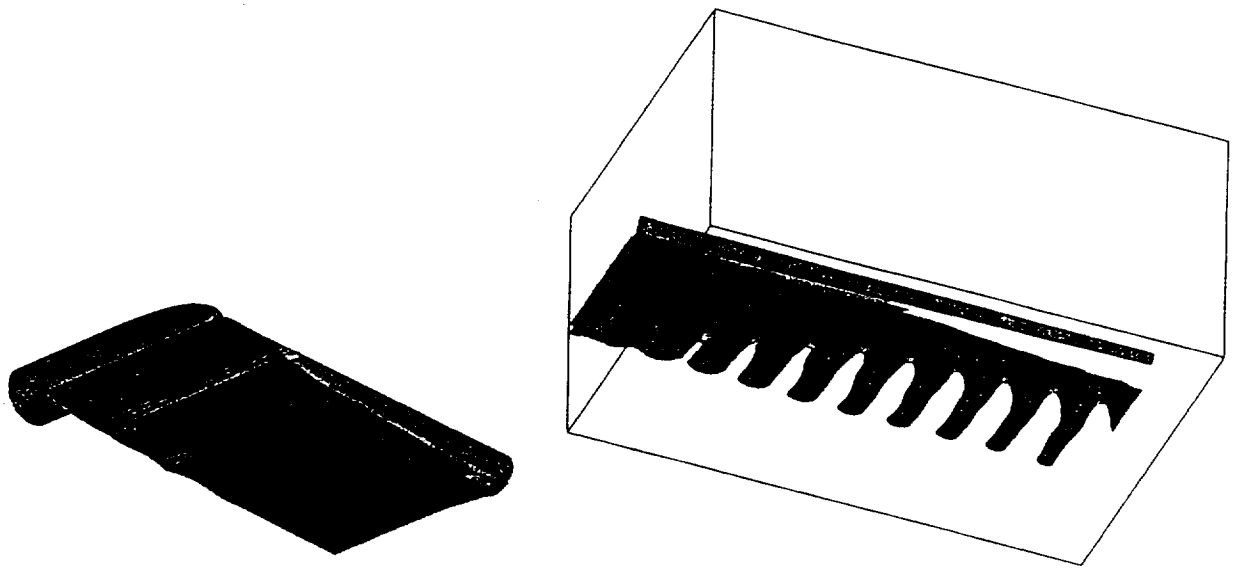

Figure 10. Flow past wings in tandem. Left: iso-surfaces for the streamwise component of the velocity for the leading wing (corresponding 97.5% of the free-stream value). Right: iso-surfaces for the wake region; streamwise and spanwise components of the vorticity (corresponding to 0.5 value).

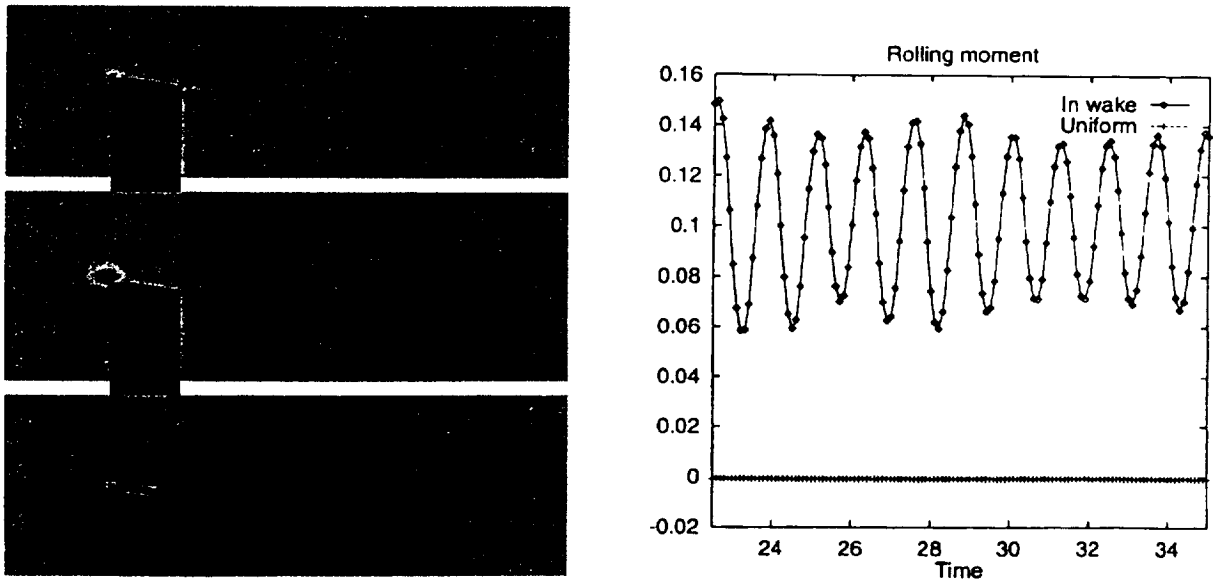

Figure 11. Flow past wings in tandem. Left: vertical component of the velocity at three vertical planes: the right wing tip, the center, and the left wing tip. Right: rolling moment for the trailing wing, compared to the case when that wing is in a uniform flow field.